Structure and Dynamics of Molten AgCl. The Inclusion of Induced Polarization

Joaquim Trullàs* and Olga Alcaraz

Departament de Física i Enginyeria Nuclear, Universitat Politècnica de Catalunya, Mòdul B4 Campus Nord UPC, 08034 Barcelona, Spain

Luis Enrique González

Departamento de Física Teórica, Facultad de Ciencias, Universidad de Valladolid, 47011 Valladolid, Spain

Moises Silbert

School of Chemical Sciences, University of East Anglia, Norwich NR4 7TJ, U.K.

Received: May 15, 2002; In Final Form: October 9, 2002

Three sets of molecular dynamics simulations have been carried out to study the static structure and transport properties of molten AgCl at 1073 K. The first uses the Vashishta−Rahman rigid-ion potential (R-VR). The other two are polarizable ion potentials, which consist of the Vashishta−Rahman (P-VR) or the Born−Mayer (P-BM) rigid-ion potentials to which the anion-induced dipole polarization contributions are added. Both polarized model potentials reproduce well the main features of the structure of molten AgCl, including the characteristic three-peak feature present in the experimental broad principal peak of its total structure factor; this is not present in the R-VR simulations. The two polarized model potentials differ significantly in the way they account for the transport properties of the melt, by the mean square displacements, the velocity correlation functions, self-diffusion coefficients, or the ionic conductivity. In the case of the latter, the experimental result ($\sigma = 4.7$ $(\Omega\cdot\text{cm})^{-1}$) is bracketed between the R-VR ($\sigma = 5.8$ $(\Omega\cdot\text{cm})^{-1}$) and the P-VR ($\sigma = 4.0$ $(\Omega\cdot\text{cm})^{-1}$) values, with the P-BM value ($\sigma = 1.3$ $(\Omega\cdot\text{cm})^{-1}$) significantly lower.

1. Introduction

This paper is concerned with the structure and ionic transport properties of molten AgCl near melting. A few years ago we reported the results of calculations for molten AgBr and AgCl using the hypernetted chain theory of liquids and molecular dynamics (MD) simulations.[1] The potentials used in these calculations were rigid potentials with the functional form originally proposed by Vashishta and Rahman[2] (VR) for α-AgI. The results in ref 1 for the total static structure factor $S_T(k)$ are in good qualitative agreement with the available experimental neutron scattering data.[3−5] Those calculations predict, in agreement with experiment, that the average coordination number between unlike ions is nearer to four than the value of six expected from their rock salt solid-state structure. We recall that Andreoni and Tosi,[6] and later Nield et al.,[7] suggested that melting frustrates a possible diffuse transition of these systems to a superionic state. This is a possible explanation for the change in the average coordination number on melting.

However, the results reported in ref 1 failed to reproduce the characteristic three-peak structure present in the principal peak of the experimental $S_T(k)$. On the other hand, Wilson et al.[8] (WMCC) claimed that, in their simulations of AgCl, the three-peak structure can only be predicted when polarizable, rather than rigid, ionic potentials are used. Madden and co-workers have, for some years, suggested that the unusual structural properties in materials, which, on electronegativity grounds, may be expected to be ionic, can be shown to be a consequence of polarization effects.[9] Their proposition has made possible the advance in our understanding of the rich variety in structural behavior of a wide range of molten salts. In the case of AgCl, WMCC suggested that this system is highly dipole- and quadrupole-polarizable.

While we share the view of Madden and co-workers, we were concerned at the necessity of including induced quadrupole polarization effects in accounting for the behavior of $S_T(k)$ in molten AgCl. One of the aims of this work is to find out whether it is possible to account for the properties of molten AgCl, attributed to the contributions of the induced polarization to the potentials of interaction, using only the dipole-induced contributions. Whereas induced quadrupole polarization effects are first order in the low-temperature solid state, because the cubic symmetry of the rock salt crystalline structure of AgCl will cancel out the induced dipole contributions, we suggest they become second-order effects in the liquid state. Actually, in ref 8 there are already indications that appear to confirm our suggestions.

We have another, practical, concern. WMCC carried out their simulations with 216 ions. To obtain accurate results at low k, they calculated $S_T(k)$ directly in reciprocal space up to 2.2 Å^{-1}. For $k \geq 2.2$ Å^{-1} they evaluated $S_T(k)$ by Fourier transforming the pair distribution functions $g_{ab}(r)$. The problem of concern here is that the middle peak of the three-peak feature is precisely in the region where the direct calculations and the Fourier transformation are matched. Since the orthonormality condition between real and reciprocal space is, in their simulations, $\Delta k \Delta r \approx 0.03$, it raises questions as to whether the middle peak, absent when using rigid ion potentials, is indeed present or is an artifact of the computational procedure used to Fourier transform

* Corresponding author. E-mail: quim.trullas@upc.es.

10.1021/jp026118e CCC: $25.00
Published on Web 12/05/2002

$g_{ab}(r)$. Last but not least, we present here the first simulation results for the ionic transport properties of molten AgCl that include induced polarization effects.

The polarized ion potentials are constructed by adding the dipole-induced polarization effects to appropriately chosen rigid-ion model (RIM) potentials. Here we use both the Born−Mayer (BM),[10] used by WMCC, and the VR forms. The dipole-induced polarization contributions to the potentials used below mirror those developed by González et al.[11] for liquid metals and charge-stabilized colloidal dispersions and are also similar to the approach used by Madden and co-workers in their studies of 3:1 molten salts.[12] Hence, the polarizable part of the potentials is not the same as those used by WMCC but, as noted in ref 12, the approach used in this work is more consistent and applicable to the whole range of molten salts. We discuss this formalism in some detail in section 2, where we also write down the RIM potentials.

The simulations presented in this work for molten AgCl compare the results of using both polarizable ion potentials, at a thermodynamic state where both exhibit a liquid phase. However, we only present the results for the VR rigid ion potential, as the BM rigid ion potential does not melt at this thermodynamic state.

In section 3 we define the properties we calculate. These include the static structure and ionic transport properties. We have already reported[13] the results for the total structure factor $S_T(k)$ and the Bhatia−Thornton partial structure factors.[14] However, in the present work we analyze carefully the results obtained for the pair distribution functions $g_{ab}(r)$ and the Ashcroft−Langreth (AL) partial structure factors $S_{ab}(k)$.[14] Moreover, we investigate carefully the contributions that make up the broad principal peak in the total structure factor $S_T(k)$ of molten AgCl by analyzing the results for the weighted AL partial structure factors $\bar{S}_{ab}(k)$. We specifically show that the induced polarization contribution is indispensable in accounting for the middle peak of the three-peak feature in the principal peak of $S_T(k)$. We include, for completeness, a comparison between the simulated and experimental results for $S_T(k)$. We also report the first results obtained for the mean square displacements $\langle r_a^2(t)\rangle$, the velocity autocorrelation functions $\Lambda_a(t)$, the distinct correlation function $\Lambda^d(t)$, the diffusion coefficients D_a, and the specific ionic conductivity σ using polarizable ion potentials for molten AgCl, and we are specifically concerned with the effects these potentials have on the transport properties. We actually show that their inclusion promotes further the mobility of the cations in a manner akin to the behavior found in superionic melts. The results of our simulations are presented in section 4.

2. Potentials

We denote by R-VR the rigid ion model pair potentials based on the functional form originally proposed by Vashishta and Rahman,[2] namely

$$\phi_{ab}^{VR}(r) = \frac{z_a z_b e^2}{r} + \frac{A(\sigma_a + \sigma_b)^6}{r^6} - \frac{P_{ab}}{r^4} - \frac{C_{ab}}{r^6} \qquad (2.1)$$

The first term on the rhs of eq 2.1 models the Coulomb interaction between the effective, namely fractional, charges; the second term models the repulsion between the ions arising from the overlap of the outer shell of electrons; the third is the effective monopole-induced dipole attractive interaction, and the last is the dispersion or van der Waals contribution. It would appear that these fractional charges and the third term somehow mimic crudely, and incompletely, induced polarization effects.

The rigid BM model pair potentials that we denote as R-BM are given by[10]

$$\phi_{ab}^{BM}(r) = \frac{z_a z_b e^2}{r} + B_{ab}\exp(-a_{ab}r) - \frac{C_{ab}}{r^6} \qquad (2.2)$$

For the R-VR potential we used the parametrization given in ref 1, and for the R-BM potential, we used those given in ref 8. Two points need to be mentioned. The first is that in the VR potentials the effective charges $|z| = 0.68$ are used, while the BM potentials use formal charges $|z| = 1$. The second is that, in the VR potentials, the anionic radius is about twice the cationic radius, $\sigma_- \cong 2\sigma_+$, while in the BM potentials $a_{--} \cong a_{++}$.

The polarizable contributions are added to the RIM potentials, with one omission in the R-VR, as follows. We assume that a polarizable ion placed at position $\mathbf{r}_i$ experiences, in a system of N polarizable ions, an induced dipole moment $\mathbf{p}_i$ in response to the electric field $\mathbf{E}_i$ due to all other ions, given by the linear approximation

$$\mathbf{p}_i = \alpha_i \mathbf{E}_i \qquad (2.3)$$

where α_i is the polarizability of the ion. The field at $\mathbf{r}_i$ is

$$\mathbf{E}_i = \mathbf{E}_i^q + \mathbf{E}_i^p = \sum_{\substack{j=1\\ j\neq i}}^{N} \frac{q_j}{r_{ij}^3}\mathbf{r}_{ij} + \sum_{\substack{j=1\\ j\neq i}}^{N}\left(3\frac{(\mathbf{p}_j\cdot\mathbf{r}_{ij})}{r_{ij}^5}\mathbf{r}_{ij} - \frac{1}{r_{ij}^3}\mathbf{p}_j\right) \qquad (2.4)$$

where $\mathbf{E}_i^q$ denotes the field at $\mathbf{r}_i$ due to all the point charges except $q_i = z_i e$, and $\mathbf{E}_i^p$ denotes the field at $\mathbf{r}_i$ due to all the dipole moments except $\mathbf{p}_i$, and $\mathbf{r}_{ij} = \mathbf{r}_i - \mathbf{r}_j$ with r_{ij} its modulus.

The induced polarization contributions to the potential energy may be written as[15]

$$U^{ind} = U^{qp} + U^{pp} + U^{self} = -\sum_{i=1}^{N}\mathbf{p}_i\cdot\mathbf{E}_i^q - \left(\frac{1}{2}\right)\sum_{i=1}^{N}\mathbf{p}_i\cdot\mathbf{E}_i^p + \sum_{i=1}^{N}\frac{p_i^2}{2\alpha_i} \qquad (2.5)$$

where U^{qp} is the energy contribution of the charge−dipole interactions, U^{pp} the energy of the dipole−dipole interactions, and U^{self} denotes the self-energy contribution, which corresponds to the energy required in creating the N induced dipoles.

We have used two polarizable potentials in this work. In both cases the induced polarization contributions, eq 2.5, are simply added to the rigid-ion potentials. The first, which we call the polarizable Vashishta−Rahman (P-VR), includes the R-VR pair potential, eq 2.1, with the omission of the effective monopole-induced dipole term ($-P_{ab}/r^4$). The second, which we call the polarizable Born−Mayer (P-BM), includes the R-BM pair potential. In the P-VR potential, we use for the anion polarizability, as in ref 1, the value $\alpha_- = 3.45$ Å^3, while, in the P-BM potential, we follow WMCC in using for the anion polarizability the value $\alpha_- = 3.08$ Å^3.

In carrying out the MD simulations, we actually have to calculate the forces. This is done taking into account that the dipole moments adjust themselves to minimize U^{ind}; namely, eq 2.3 implies $\partial U^{ind}/\partial \mathbf{p}_j = 0$. Although the dipole moments are determined by the field, and therefore depend on the ionic positions, the gradient calculations are simplified by the

minimization condition, which implies that only explicit derivatives of U^{ind} with respect to the coordinates have to be considered. Then the induced force acting on the ion i can be written as

$$\mathbf{F}_i^{\mathrm{ind}} = \mathbf{F}_i^{qp} + \mathbf{F}_i^{pp} \tag{2.6}$$

where

$$\mathbf{F}_i^{qp} = q_i \mathbf{E}_i^p - \sum_{\substack{j=1 \\ j\neq i}}^{N} q_j \left(3\frac{(\mathbf{p}_i \cdot \mathbf{r}_{ij})\mathbf{r}_{ij}}{r_{ij}^{\,5}} - \frac{\mathbf{p}_i}{r_{ij}^{\,3}} \right) \tag{2.7}$$

is the sum of the force acting on the point charges q_i due to the other point dipoles and the force acting on $\mathbf{p}_i$ due to the other point charges, and

$$\mathbf{F}_i^{pp} = \sum_{\substack{j=1 \\ j\neq i}}^{N} \left(-15\frac{(\mathbf{p}_i \cdot \mathbf{r}_{ij})(\mathbf{p}_j \cdot \mathbf{r}_{ij})\mathbf{r}_{ij}}{r_{ij}^{\,7}} + 3\frac{(\mathbf{p}_i \cdot \mathbf{r}_{ij})\mathbf{p}_j}{r_{ij}^{\,5}} + 3\frac{(\mathbf{p}_j \cdot \mathbf{r}_{ij})\mathbf{p}_i}{r_{ij}^{\,5}} + 3\frac{(\mathbf{p}_i \cdot \mathbf{p}_j)\mathbf{r}_{ij}}{r_{ij}^{\,5}} \right) \tag{2.8}$$

is the force acting on $\mathbf{p}_i$ due to the other dipoles.

3. Properties

The basic structural properties evaluated in the simulations are the partial radial distribution functions $g_{ab}(r)$ and the Ashcroft−Langreth (AL) partial structure factors $S_{ab}(k)$. Assuming a 1:1 system, both are related by the Fourier transform

$$S_{ab}(k) = \delta_{ab} + \frac{\rho}{2}\int_0^\infty [g_{ab}(r) - 1]\,\frac{\sin kr}{kr} 4\pi r^2\,\mathrm{d}r \tag{3.1}$$

where ρ denotes the total ionic number density of the melt. In the MD simulations it is possible to evaluate $S_{ab}(k)$ directly by using

$$S_{ab}(k) = \frac{2}{N}\Big\langle \sum_{ia=1}^{Na} \exp(i\mathbf{k}\cdot\mathbf{r}_{ia}) \sum_{jb=1}^{Nb} \exp(-i\mathbf{k}\cdot\mathbf{r}_{jb}) \Big\rangle \tag{3.2}$$

where the angular brackets denote the ensemble average over the equilibrium configurations and $\mathbf{k} = (2\pi/L)\mathbf{n}$ is the wave vector in the reciprocal space allowed by the periodic boundary conditions, with $\mathbf{n}$ a vector with integer components and $L = (N/\rho)^{1/3}$ the cubic box side ($N = N_+ + N_-$). Actually we adopt a hybrid method for the evaluation of $S_{ab}(k)$ that we describe in the Results section.

We now turn to the ionic transport properties.[16,17] These include the main body of results of this work. We have computed the mean square displacements

$$\langle r_a^{\,2}(t)\rangle = \frac{1}{3}\frac{1}{N_a}\sum_{ia=1}^{Na} \langle |\mathbf{r}_{ia}(t) - \mathbf{r}_{ia}(0)|^2 \rangle \tag{3.3}$$

and the velocity autocorrelation functions (vacf)

$$\Lambda_a(t) = \frac{1}{3}\frac{1}{N_a}\sum_{ia=1}^{Na} \langle \mathbf{v}_{ia}(t)\cdot\mathbf{v}_{ia}(0)\rangle \tag{3.4}$$

from which the normalized vacf reads

$$C_a(t) = \frac{\Lambda_a(t)}{\Lambda_a(0)} = \frac{m_a}{k_{\mathrm{B}}T}\Lambda_a(t) \tag{3.5}$$

The charge−current density autocorrelation function reads, assuming $|z_a| = 1$,

$$\Lambda^Z(t) = \frac{1}{3}\frac{1}{N}\Big\langle \Big(\sum_{i=1}^{N} z_i \mathbf{v}_i(t)\Big)\cdot\Big(\sum_{i=1}^{N} z_i \mathbf{v}_i(0)\Big)\Big\rangle = \frac{1}{2}[\Lambda_+(t) + \Lambda_-(t)] + \frac{1}{4}\Lambda^{\mathrm{d}}(t) \tag{3.6}$$

where $\Lambda^{\mathrm{d}}(t)$, the distinct correlation function, arises from the cross-correlations between two different ions. The normalized distinct correlation function reads

$$\delta(t) = \frac{1}{4}\frac{\Lambda^{\mathrm{d}}(t)}{\Lambda^Z(0)} = \frac{m_- m_+}{2(m_+ + m_-)}\Lambda^{\mathrm{d}}(t) \tag{3.7}$$

The transport coefficients in which we are interested are the self-diffusion coefficients D_a, which we calculate using both the Einstein relation and the Kubo formula, namely

$$D_\alpha = \lim_{t\to\infty}\frac{\langle r_a^{\,2}(t)\rangle}{2t} \quad \text{and} \quad D_a = \int_0^\infty \Lambda_a(t)\,\mathrm{d}t \tag{3.8}$$

and the ionic conductivity, for which we also use the corresponding Kubo formula,

$$\sigma = \frac{\rho e^2}{k_{\mathrm{B}}T}\int_0^\infty \Lambda^Z(t)\,\mathrm{d}t = \sigma_{\mathrm{NE}}(1 - \Delta) \tag{3.9}$$

where σ_{NE} denotes the ionic conductivity in the Nernst−Einstein approximation

$$\sigma_{\mathrm{NE}} = \frac{\rho e^2}{k_{\mathrm{B}}T}\frac{1}{2}(D_+ + D_-) \tag{3.10}$$

and Δ, a measure of the deviation from σ_{NE}, is related to the distinct correlation function by

$$\Delta = \frac{-1}{2(D_+ + D_-)}\int_0^\infty \Lambda^{\mathrm{d}}(t)\,\mathrm{d}t \tag{3.11}$$

4. Results

We have carried out MD simulations in a system made up of 500 cations and 500 anions placed in a cubic box with periodic boundary conditions, at $\rho = 0.0384$ ions/Å^3 and $T = 1073$ K. The positions and velocities of the ions have been computed using the Beeman's integration algorithm with a time step of 5×10^{-15} s. Both the Coulomb and induced polarization contributions are long-range interactions. In both cases the Ewald summation method has been used. To keep continuity in the present discussion, details of the Ewald sum algorithm used in our simulations are given in the Appendix.

Care must also be taken in the evaluation of the induced polarization contributions. It is important to realize that $\mathbf{p}_i$ is determined by $\mathbf{E}_i$, which comes from the contributions of the charges of all the other ions and all the other induced moments, which themselves are determined by the fields at the positions of the other ions. We therefore find that $\mathbf{E}_i$, and consequently $\mathbf{p}_i$, depends on the field at the positions of all the other ions

through the field created by all the dipole moments including $\mathbf{p}_i$. For given ionic positions $\{\mathbf{r}_j\}$, the evaluation of $\mathbf{p}_i$ and $\mathbf{E}_i$ can be achieved by a simple prediction−correction iterative procedure.[18] As starting values, one may choose as the predicted field $\mathbf{E}_i^p* = 0$. A more suitable choice in molecular dynamics calculations is the vector $\mathbf{E}_i^p$ at the previous time step. Then, the following iterative procedure is repeated until convergence is reached:

(1) From the predicted dipole field, $\mathbf{E}_i^p*$, evaluate the dipole moment $\mathbf{p}_i* = \alpha_i(\mathbf{E}_i^q + \mathbf{E}_i^p*)$.

(2) From $\{\mathbf{p}_j*\}$ evaluate the corrected dipole field $\mathbf{E}_i^{p\dagger} = \mathbf{E}_i^p(\{\mathbf{r}_j\},\{\mathbf{p}_j*\})$, eq 2.4.

(3) Repeat step 1 with $\mathbf{E}_i^p* = \mathbf{E}_i^{p\dagger}$ until $\sum|\mathbf{E}_i^{p\dagger} - \mathbf{E}_i^p*|^2/|\mathbf{E}_i^{p\dagger}|^2$ is small enough ($\approx 10^{-3}$).

For the systems under study the initial conditions in the equilibration process are important, and it is essential to start with an initial configuration in which the anions exhibit liquid behavior. We chose a distorted rock salt crystalline structure at a density ρ smaller than and at a temperature T higher than the density and temperature of interest, so that ions diffuse more rapidly, thus ensuring that equilibrium was achieved in a relatively short time. Once equilibrium was reached, we compressed and cooled the system in several steps, making sure that at each step the liquid behavior was preserved, until the density and temperature of interest. It is worth mentioning that the equilibration process required long simulations (about 300 000 time steps) to make sure that the system did not quench into a solid phase, as it did when the R-BM potential model was used.

We have studied molten AgCl by using a simple rigid-ion model (R-VR) and the two polarizable ion models (P-VR and P-BM) presented in section 2. For the reasons given above, we were not able to study the R-BM potential. We have also attempted to study the P-VR potentials model assuming that *both* anions and cations are polarizable (using $\alpha_+ = 1.72$ Å^3, as in ref 10). We found that this model leads to the polarization catastrophe, namely ions approach each other too much. We conjecture that a similar effect will be found using the P-BM potential. The fact that correct results are only obtained when the polarization of the cations is altogether ignored is a moot point in need of further work.

A. Liquid Structure. The results for the pair distribution functions $g_{ab}(r)$ are presented in Figure 1. It is interesting to note that, although we only take into account the anion polarizability, it is mainly the cations that are affected by the induced polarization interactions. The same comment applies to practically all of the properties studied in this work.

The main effects on the cations structure due to the anion polarizability are the following: (i) the cationic charge penetration increases in going from the R-VR to the P-VR potentials, specifically the penetration of the low r tail of $g_{++}(r)$ beneath the principal peak of $g_{+-}(r)$; (ii) $g_{++}(r)$ exhibits less structure than the R-VR, although the dampening in oscillations is less when the P-BM potential is used; (iii) a shoulder, or not well developed second peak, appears in $g_{++}(r)$ between the first and second peaks of $g_{+-}(r)$; and (iv) the characteristic charge ordering present in simple molten salts is broken. These features are indicative of the behavior present in the superionic melts and supports the conjectures discussed in ref 1. Moreover, this is indicative of changes in the mobility of the cations, and we show below that this is indeed the case.

From the $g_{+-}(r)$ we have estimated the coordination numbers n_{+-} by carrying out the integration up to the first minimum of $4\pi r^2 g_{+-}(r)$. The values found, when the polarization potentials are used, are 5.1 (P-VR) and 5.3 (P-BM), a small increase on the R-VR value.[1]

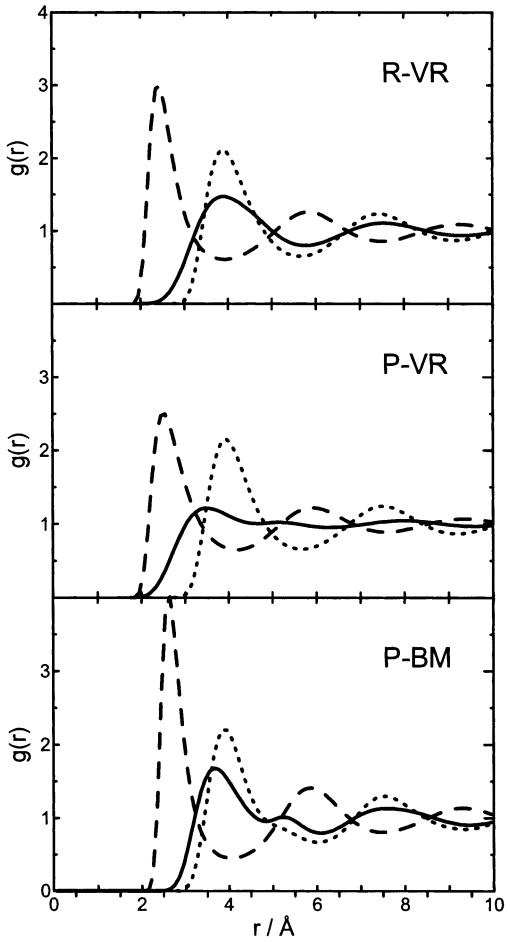

Figure 1. MD simulations for the pair distribution functions $g_{ab}(r)$ of molten AgCl at $\rho = 0.0384$ ions/Å^3 and $T = 1073$ K, using the following potentials: R-VR (top), P-VR (middle), and P-BM (bottom). Key: (solid line) $g_{++}(r)$; (dotted line) $g_{--}(r)$; (dashed line) $g_{+-}(r)$.

We now turn to the AL partial structure factors defined by eqs 3.1 and 3.2. To minimize the problems caused by the use of periodic boundary conditions, we have evaluated $S_{ab}(k)$ by a hybrid method.[8] For k beyond 4 Å^{-1}, we have evaluated eq 3.1 up to $L/2$ instead of ∞. At low k this method gives spurious oscillations due to truncation errors, and therefore we have computed $S_{ab}(k)$ directly, up to 4 Å^{-1} and slightly beyond, by using eq 3.2. The results are shown in Figure 2.

The most salient differences, on comparing the results obtained from using the R-VR and P-VR potentials, are in $S_{++}(k)$. In the latter the height of the principal peak is lower than that using R-VR, and a shoulder, or second peak, appears at around 2.4 Å^{-1}. We believe that its presence is decisive in accounting for the three-peak feature in the total structure factor (see below). Moreover, both the depth of the first minimum in $S_{--}(k)$ is shallower, and the height of the principal peak of $S_{+-}(k)$ is lower, when the P-VR potential is used; there is also a shift toward lower values of k in the principal peak of $S_{+-}(k)$, and of the first minimum of $S_{--}(k)$ in the P-VR results relative to those obtained with the R-VR potential.

The principal peaks of the like partials are higher when the P-BM potential is used as compared to the P-VR, and the minimum of the unlike partial is deeper. Moreover, the second peak in $S_{++}(k)$ is also present, and the oscillations are more pronounced, for the P-BM potential as compared to the P-VR. This is due to the P-BM potential having a more repulsive ion

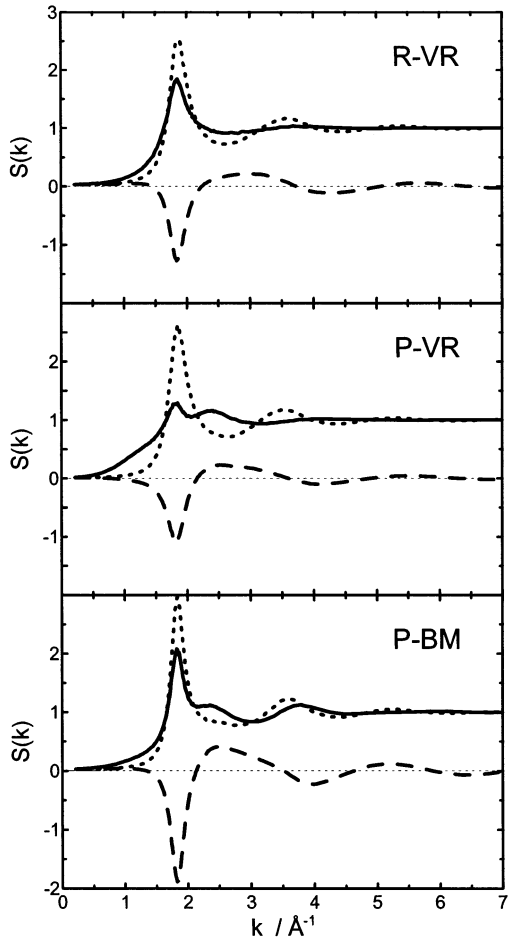

Figure 2. MD simulations for the Ashcroft−Langreth (AL) partial structure factors $S_{ab}(k)$ of molten AgCl at $\rho = 0.0384$ ions/Å^3 and $T = 1073$ K, using the following potentials: R-VR (top), P-VR (middle), and P-BM (bottom). Key: (solid line) $S_{+\,+}(k)$; (dotted line) $S_{-\,-}(k)$; (dashed line) $S_{+\,-}(k)$.

core than the P-VR, in agreement with the remarks made by WMCC. The preceding observations are consistent with comments made above on the $g_{ab}(r)$.

To clarify how the combination of the three partial structure factors produces the characteristic three-peak feature present in the experimental $S_T(k)$, we have also calculated the weighted AL partial structure factors, which are defined as

$$\bar{S}_{ab}(k) = \frac{b_a b_b}{(b_a^{\,2} + b_b^{\,2})} S_{ab}(k) \qquad (4.1)$$

where the neutron scattering lengths for normal isotopic composition of the ions are $b_{Ag}^{nat} = 5.922$ fm and $b_{Cl}^{nat} = 9.577$ fm.[19] The scattering lengths are the weighting factors and, to a large extent, are responsible for whether such a feature is present in the experimental data. Moreover, the features we are concerned with are mainly restricted to the rather narrow range of values between 1.75 and 3.75 Å^{-1}, the approximate span of the broad principal peak in molten AgCl. Our results are shown in Figure 3, where we plot $\bar{S}_{+\,+}(k)$, $(\bar{S}_{-\,-}(k) + \bar{S}_{+\,-}(k))$, and also the calculated

$$S_T(k) = \bar{S}_{+\,+}(k) + (\bar{S}_{-\,-}(k) + \bar{S}_{+\,-}(k)) \qquad (4.2)$$

for comparison. The second term on the right hand side is taken in this manner so that we can look at the combined contributions of the two weighted partials, as they tend to partially cancel

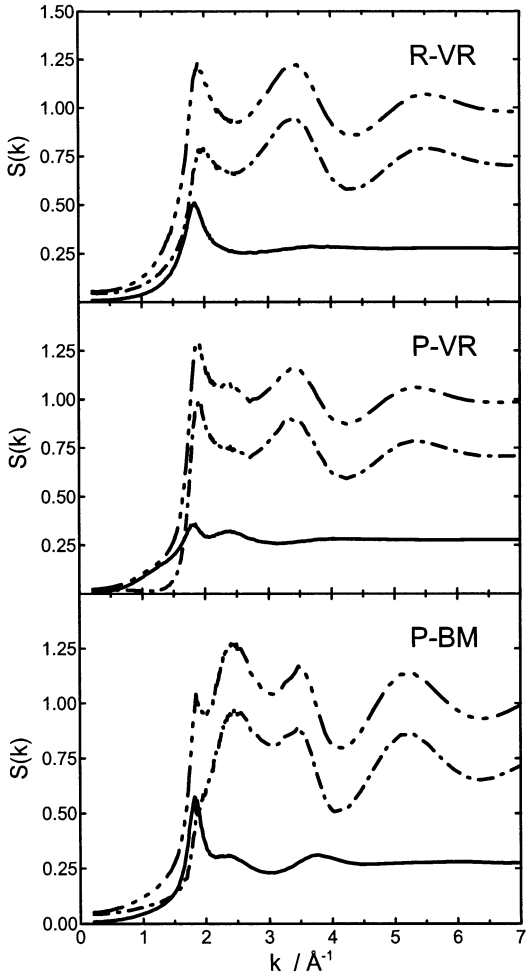

Figure 3. MD simulations of molten AgCl at $\rho = 0.0384$ ions/Å^3 and $T = 1073$ K. Weighted AL partial structure factors, $\bar{S}_{+\,+}(k)$ and $(\bar{S}_{-\,-}(k) + \bar{S}_{+\,-}(k))$, and total static structure factor, $S_T(k)$, using the following potentials: R-VR (top), P-VR (middle), and P-BM (bottom). Key: (solid line) $\bar{S}_{+\,+}(k)$; (dash−dotted line) $(\bar{S}_{-\,-}(k) + \bar{S}_{+\,-}(k))$; (dash−3-dots line) $S_T(k)$.

each other. Contrasting the rigid-ion results with the polarizable-ion results, it is clear that the induced polarization contributes to the middle peak—absent in the rigid ion $S_T(k)$—in two ways: first because of the shoulder that appears in $(\bar{S}_{-\,-}(k) + \bar{S}_{+\,-}(k))$—very clear using the P-BM potentials but rather weak using the P-VR potentials—and second because of the presence of the shoulder, or second peak, in $\bar{S}_{+\,+}(k)$.

We include for completeness, in Figure 4, the results for $S_T(k)$, comparing the experimental neutron diffraction data[3,4] with the results, shown in Figure 3, obtained by using both the P-BM and P-VR potentials. These results have already been presented in ref 13. We add here the following comments. The simulated results, for the polarized potentials, exhibit the three characteristic peaks at slightly different positions and bracketed by the two sets of experimental data. With the P-VR potential the peak at the lower k value is the more pronounced, with a rather weak middle peak. On the other hand, with the P-BM potential, it is exactly the opposite. The differences reflect the differences in the partial structure factors discussed above. We note that the results obtained here resemble those obtained in ref 8, with the advantage that the use of a larger number of particles gives us more confidence in our results.

B. Transport Properties. We now turn to the transport properties. Figure 5 shows the results for the mean square displacements $\langle r_a^2(t)\rangle$. We note that, when the P-VR potential

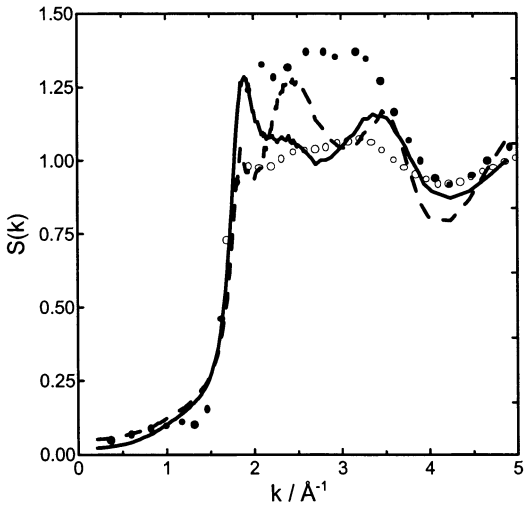

Figure 4. Total static structure factor, $S_T(k)$, of molten AgCl at $\rho = 0.0384$ ions/Å^3 and $T = 1073$ K obtained by MD simulations using the following potentials: (solid line) P-VR and (dashed line) P-BM. Neutron diffraction data at the same thermodynamic state from (full circles) ref 4 and from (open circles) ref 3 at 1123 K.

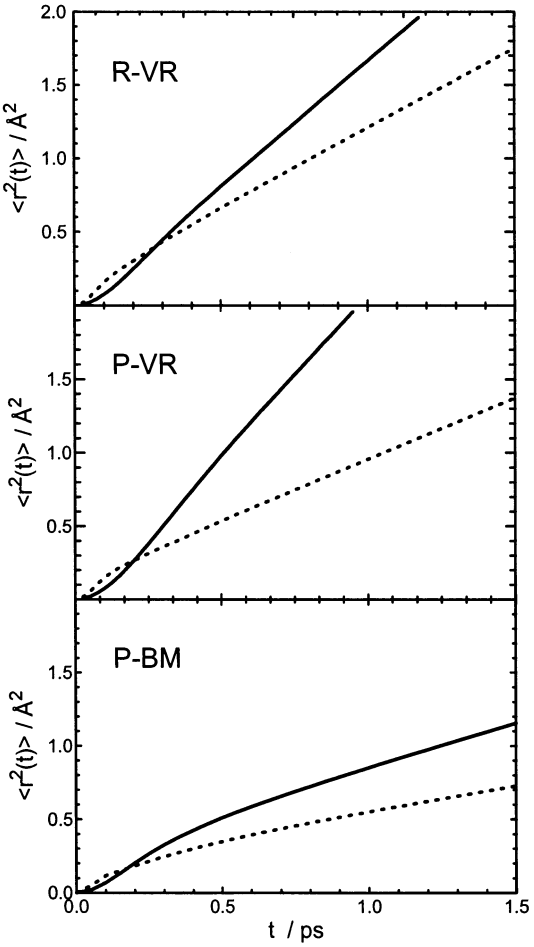

Figure 5. MD simulations for the mean square displacements, $\langle r_a^2(t)\rangle$, of molten AgCl at $\rho = 0.0384$ ions/Å^3 and $T = 1073$ K, using the following potentials: R-VR (top), P-VR (middle), and P-BM (bottom): (solid line) cations; (dotted line) anions.

is used, the cations become more, and the anions less, mobile than is the case with the R-VR potential. This, in turn, affects the values obtained for the self-diffusion coefficients, which we discuss below. It is as if when the anionic polarization is switched on, "faster" channels become available for the cations.

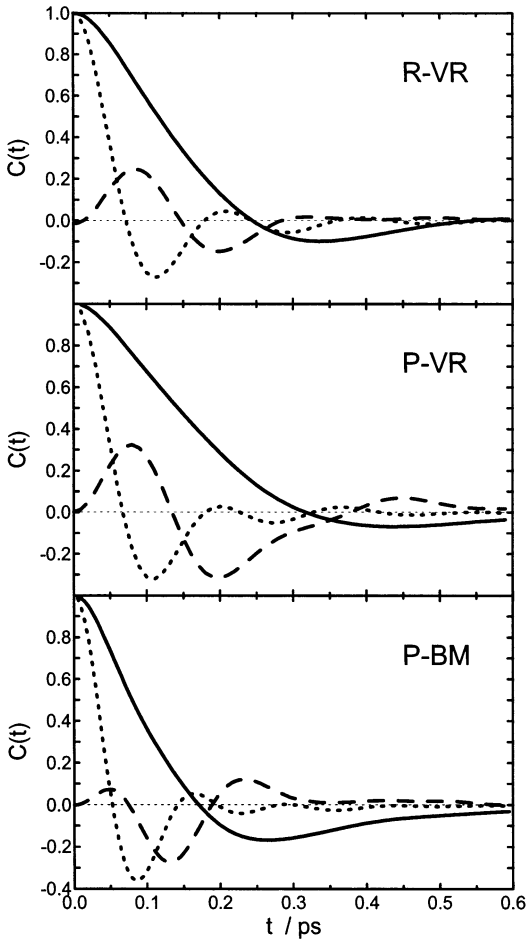

Figure 6. MD simulations for the normalized velocity autocorrelation functions, $C_a(t)$, for (solid line) cations and (dotted line) anions, and (dashed line) distinct correlation function, $\delta(t)$, of molten AgCl at $\rho = 0.0384$ ions/Å^3 and $T = 1073$ K, using the following potentials: R-VR (top), P-VR (middle), and P-BM (bottom).

The differences in slope between $\langle r_+^2(t)\rangle$ and $\langle r_-^2(t)\rangle$ are similar to those we obtained for the superionic melts.[20] We have already discussed the features observed at short times in earlier work, and we have nothing to add to those comments.[21] We are also presenting the first mean square displacements for the polarizable BM potentials, whose slopes are less pronounced than those for the VR potentials.

Figure 6 shows the normalized vacf and distinct correlation functions. The P-VR cation vacf is more diffusive; it decays more slowly at short times and its backscattering is weaker, relative to the results obtained in the R-VR case. Similarly, the anion vacf exhibits deeper backscattering and more pronounced oscillations, at a higher frequency, and the magnitude of the amplitudes of the distinct correlation function is larger. The results for the vacf are consistent with the comments made above for the mean square displacements; those for the distinct correlation function will affect the values for the ionic conductivity through Δ, as we show below.

The P-BM vacf and distinct correlation functions are also presented for the first time. The P-BM cation vacf decays faster and its backscattering is deeper when compared to the VR models. Moreover, the anion vacf and the distinct correlation function oscillate at a higher rate. This picture is consistent with comments made above on the structural properties and the mean square displacements.

In Table 1 we show the results for the diffusion coefficients and the conductivity of molten AgCl. The cation P-VR diffusion

TABLE 1: Transport Properties of Molten AgCl at ρ = 0.0384 ions/Å^3 and T = 1073 K[a]

	R-VR	P-VR	P-BM	exp[22]
$D_+/(10^{-5}$ cm^2/s)	8.55	10.4	2.85	
$D_-/(10^{-5}$ cm^2/s)	5.45	4.1	1.65	
$\sigma/((\Omega\cdot$cm$)^{-1})$	5.8	4.0	1.3	4.7
Δ	−2.4	0.17	0.15	

[a] D_a denotes the diffusion coefficients, σ the ionic conductivity, and Δ the deviation from the Nernst−Einstein approximation, eq 3.9. The first three columns give the MD simulation results using the R-VR, P-VR, and P-BM potentials. Column four quotes the experimental value for the ionic conductivity.

constant is larger, and the anion smaller, than the corresponding R-VR values; with the P-BM results, as anticipated, very much smaller in both cases. Although there are no experimental data on the diffusion constants for molten AgCl, we believe that, when those measurements are made at the thermodynamic state studied in this work, their values will be bracketed by the R-VR and P-VR obtained in this work. We base our conjecture on the results obtained for the conductivity, that we discuss below. We note that the P-BM results for the self-diffusion coefficients at 1073 K are close to those reported by WMCC[8] for the model that only includes the anion-induced dipole polarization with the values (in units of 10^{-5} cm^2/s) $D_+ = 3.62$ and $D_- = 2.49$, as well as in the model that also includes quadropole polarization, $D_+ = 3.46$ and $D_- = 2.60$, both at 1123 K.

We carried out the conductivity calculations using the formal charge $|z_a| = 1$. Our reasons, which only apply to the VR potentials, are as follows.[1] Whereas, in their interactions we assume the ions only "see" effective charges, which we tentatively attribute to an average screening effect of the electronic shells, in their transport the charges carry with them the full complement of electrons. This dichotomy in the values used for the charges is empirical and in need of theoretical justification. Our results show that the experimental value[22] of σ is bracketed between the R-VR and the P-VR results; with probably the latter marginally in better agreement with experiment. The P-BM result is significantly lower than experiment.

Departures from the Nernst−Einstein relation, namely the parameter Δ, are also shown in Table 1. These results are very interesting, for there is a change in sign in going from the R-VR to the P-VR values. The present results reverse the systematic negative values of Δ obtained in our previous calculations for superionic melts using the R-VR potentials.[20] However, returning to Figure 6, we note that in all cases $\delta(t)$ starts from zero to positive values, larger in the VR cases than the P-BM potential. This differs from similar calculations carried out for alkali halide like melts, where $\delta(t)$ always starts from zero to negative values.[23]

Our results show that the values for Δ obtained using P-VR and P-MB are close. The sign of Δ depends on the area under the integrand of eq 3.11, and its value depends on the value of the integral and the ionic diffusion coefficients; it is the combination of the two contributions that leads to similar values of Δ for the two polarizable potentials.

5. Discussion

We have presented the details of three sets of molecular dynamics simulations: one with rigid ion potentials (R-VR) and the other two allowing the inclusion of induced dipole polarization effects in the interionic interactions in order to study the structure and transport properties of molten AgCl. In these two cases we have used the same polarization scheme, which is added to two different rigid-ion potentials, the R-VR and the R−BM potentials.

The R-VR results give a good first approximation to both the structure and ion transport properties.[1] In particular, it provides a good upper bound to the ionic conductivity. However, it fails to reproduce the characteristic three-peak structure present in the principal peak of the experimental $S_T(k)$.

The inclusion of the induced polarization effects corrects this deficiency. Very little separates the simulations of the structure using the two polarizable potentials. The simulation results are bracketed by the two sets of experimental data that we used for comparison, and until this difference in the experimental data at the level of the broad principal peak is resolved, there is no more we can add. Two further comments are in order. First, within the induced polarization scheme we have used in this work, the inclusion of the induced dipole polarization effects is sufficient to reproduce the three-peak feature in the principal peak. Second, in the simulations, this feature is not an artifact of the hybrid Fourier transform procedure used to evaluate $S_{ab}(k)$.

The differences between the two polarizable potentials also appear in the simulation results of the ion transport properties, specifically the self-diffusion constants and the ionic conductivity. The diffusion constants have smaller values, and their differences are also smaller, when the P-BM is used. The P-VR results for the conductivity are in good agreement with experimental results but not the P-BM results. Since the results for the ionic conductivity only reflect a general trend in the simulations of all the transport properties calculated in this work, we believe the apparent shortcomings of the P-BM results are probably due to the Born−Mayer rigid-ion potentials or, more precisely, to their parametrization.[24] In view of the successful results obtained for the 3:1 melts,[12] it may be useful to look again at the 1:1 molten salts using this formalism. Progress in the understanding of these systems could also come if the currently more successful semiempirical Vashishta−Rahman potentials, for the 1:1 melts, can somehow be replaced by others that, while retaining their most important features, use formal charges that are also transferable.

Acknowledgment. We thank Benedito Costa-Cabral and Mark Wilson for fruitful discussions and correspondence. This work was supported by CICYT of Spain (BFM2000-0596-CO03-02), the DURSI of the Generalitat of Catalonia (1999SGR-00146), and NATO (CRG971173).

Appendix

In carrying out MD simulations, we need to calculate the fields $\mathbf{E}_i^q$ and $\mathbf{E}_i^p$, the Coulomb and induced forces ($q_i\mathbf{E}_i^q$ and $\mathbf{F}_i^{\text{ind}}$), and the charged−charged and the induced polarization contributions to the potential energy. Their Ewald summations are given below.

Extension of the original Ewald method to a system of N point charges placed in a cubic box of side L with periodic boundary conditions allows us to write the electric potential created at any position r_0 due to all the point charges except q_i as follows

$$V_i^q(\mathbf{r}_0) = V_i^{q\mathrm{I}}(\mathbf{r}_0) + V_i^{q\mathrm{II}}(\mathbf{r}_0) + V_i^{q\mathrm{III}}(\mathbf{r}_0) \qquad \text{(A.1)}$$

$$V_i^{q\mathrm{I}}(\mathbf{r}_0) = \sum_{j=1}^{N}\sum_{\mathbf{n}'} q_j A(\beta, r_{0j\mathbf{n}}) \qquad \text{(A.2)}$$

$$V_i^{qII}(\mathbf{r}_0) = \sum_{j=1}^{N}\sum_{\mathbf{k}\neq\mathbf{0}} q_j G(\beta,k^2)\cos(\mathbf{k}\cdot\mathbf{r}_{0j}) \quad (A.3)$$

$$V_i^{qIII}(\mathbf{r}_0) = q_i\left(A(\beta,r_{0i}) - \frac{1}{r_{0i}}\right) \quad (A.4)$$

where $\mathbf{r}_{0j\mathbf{n}} = \mathbf{r}_0 - (\mathbf{r}_j + \mathbf{n}L)$, $\mathbf{n}$ are vectors with integer components, $\mathbf{k} = (2\pi/L)\mathbf{n}$ are wave vectors in the reciprocal space, $\mathbf{n}'$ under the summation sign means that $\mathbf{n} = \mathbf{0}$ must be omitted when $j = i$,

$$A(\beta,r) = \frac{\mathrm{erfc}(\beta r)}{r} \quad (A.5)$$

$$G(\beta,k^2) = \frac{4\pi}{L^3}\frac{\exp(-k^2/4\beta^2)}{k^2} \quad (A.6)$$

$\mathrm{erfc}(x) = 1 - \mathrm{erf}(x)$ is the complementary error function, and β is an adjustable parameter. Taking the negative of the gradient of eq A.1 with respect to $\mathbf{r}_0$, and particularizing the result to $\mathbf{r}_0 \rightarrow \mathbf{r}_i$, the field at $\mathbf{r}_i$ can be written as

$$\mathbf{E}_i^q = \mathbf{E}_i^{qI} + \mathbf{E}_i^{qII} \quad (A.7)$$

with

$$\mathbf{E}_i^{qI} = \sum_{j\neq i}^{N}\sum_{\mathbf{n}} q_j B(\beta,r_{ij\mathbf{n}})\mathbf{r}_{ij\mathbf{n}} \quad (A.8)$$

and

$$\mathbf{E}_i^{qII} = \sum_{\mathbf{k}\neq\mathbf{0}} G(\beta,k^2)[\sin(\mathbf{k}\cdot\mathbf{r}_i)Q_{\cos}(\mathbf{k}) - \cos(\mathbf{k}\cdot\mathbf{r}_i)Q_{\sin}(\mathbf{k})]\mathbf{k} \quad (A.9)$$

where we have omitted the terms $j = i$ in eq A.8 because their contributions cancel out,

$$B(\beta,r) = -\frac{1}{r}\frac{\mathrm{d}A(\beta,r)}{\mathrm{d}r} = \left(\frac{2\beta}{\sqrt{\pi}}\exp(-\beta^2r^2) + A(\beta,r)\right)\frac{1}{r^2} \quad (A.10)$$

$$Q_{\cos}(\mathbf{k}) = \sum_{j=1}^{N} q_j\cos(\mathbf{k}\cdot\mathbf{r}_j) \quad \text{and} \quad Q_{\sin}(\mathbf{k}) = \sum_{j=1}^{N} q_j\sin(\mathbf{k}\cdot\mathbf{r}_j) \quad (A.11)$$

Contributions from $V_i^{qIII}(\mathbf{r}_0)$ vanish because $B(\beta,r) - (1/r^3)$ goes to $-4\beta^3/(3\pi^{1/2})$ when $r \rightarrow 0$, and $\mathbf{r}_{0i}$ goes to 0 when $\mathbf{r}_0 \rightarrow \mathbf{r}_i$. Then, the force acting on q_i due to the other point charges can be evaluated by the relation

$$\mathbf{F}_i^{qq} = q_i\mathbf{E}_i^q \quad (A.12)$$

From eq A.1 the energy of the charge−charge interactions, $U^{qq} = {}^1/_2\sum_i q_i V_i^q(\mathbf{r}_i)$, can be written as

$$U^{qq} = {}^1/_2\sum_{i=1}^{N}\sum_{j=1}^{N}\sum_{\mathbf{n}'} q_i q_j A(\beta,r_{ij\mathbf{n}}) + {}^1/_2\sum_{\mathbf{k}\neq\mathbf{0}} G(\beta,k^2)[Q_{\cos}^2(\mathbf{k}) + Q_{\sin}^2(\mathbf{k})] - \frac{\beta}{\sqrt{\pi}}\sum_{i=1}^{N} q_i^2 \quad (A.13)$$

where the last term is just the limit of $V_i^{qIII}(\mathbf{r}_0)$ when $\mathbf{r}_0$ goes to $\mathbf{r}_i$. The negative of the gradient of U^{qq} with respect to an ionic position gives Ewald summations equivalent to eq A.12.

The electric potential due to a point dipole can be obtained from the potential due to a point charge by substituting q_i by $(-\mathbf{p}_i\cdot\partial/\partial\mathbf{r}_0)$. Making this substitution in eq A.1, we have

$$V_i^p(\mathbf{r}_0) = V_i^{pI}(\mathbf{r}_0) + V_i^{pII}(\mathbf{r}_0) + V_i^{pIII}(\mathbf{r}_0) \quad (A.14)$$

$$V_i^{pI}(\mathbf{r}_0) = \sum_{j=1}^{N}\sum_{\mathbf{n}'}(\mathbf{p}_j\cdot\mathbf{r}_{0j\mathbf{n}})B(\beta,r_{0j\mathbf{n}}) \quad (A.15)$$

$$V_i^{pII}(\mathbf{r}_0) = \sum_{j=1}^{N}\sum_{\mathbf{k}\neq\mathbf{0}}(\mathbf{p}_j\cdot\mathbf{k})G(\beta,k^2)\sin(\mathbf{k}\cdot\mathbf{r}_{0j}) \quad (A.16)$$

$$V_i^{pIII}(\mathbf{r}_0) = (\mathbf{p}_i\cdot\mathbf{r}_{0i})\left(B(\beta,r_{0i}) - \frac{1}{r_{0i}^3}\right) \quad (A.17)$$

Therefore, the corresponding field at $\mathbf{r}_i$ can be written as

$$\mathbf{E}_i^p = \mathbf{E}_i^{pI} + \mathbf{E}_i^{pII} + \mathbf{E}_i^{pIII} \quad (A.18)$$

$$\mathbf{E}_i^{pI} = \sum_{j=1}^{N}\sum_{\mathbf{n}'}[(\mathbf{p}_j\cdot\mathbf{r}_{ij\mathbf{n}})C(\beta,r_{ij\mathbf{n}})\mathbf{r}_{ij\mathbf{n}} - B(\beta,r_{ij\mathbf{n}})\mathbf{p}_j] \quad (A.19)$$

$$\mathbf{E}_i^{pII} = -\sum_{\mathbf{k}\neq\mathbf{0}} G(\beta,k^2)[\cos(\mathbf{k}\cdot\mathbf{r}_i)P_{\cos}(\mathbf{k}) + \sin(\mathbf{k}\cdot\mathbf{r}_i)P_{\sin}(\mathbf{k})]\mathbf{k} \quad (A.20)$$

$$\mathbf{E}_i^{pIII} = \frac{4\beta^3}{3\sqrt{\pi}}\mathbf{p}_i \quad (A.21)$$

where the terms $i = j$ cannot be omitted in eq A19,

$$C(\beta,r) = -\frac{1}{r}\frac{\mathrm{d}B(\beta,r)}{\mathrm{d}r} = \left(\frac{4\beta^3}{\sqrt{\pi}}\exp(-\beta^2r^2) + 3B(\beta,r)\right)\frac{1}{r^2} \quad (A.22)$$

$$P_{\cos}(\mathbf{k}) = \sum_{j=1}^{N}(\mathbf{p}_j\cdot\mathbf{k})\cos(\mathbf{k}\cdot\mathbf{r}_j) \quad \text{and} \quad P_{\sin}(\mathbf{k}) = \sum_{j=1}^{N}(\mathbf{p}_j\cdot\mathbf{k})\sin(\mathbf{k}\cdot\mathbf{r}_j) \quad (A.23)$$

Contributions from $V_i^{pIII}(\mathbf{r}_0)$ do not vanish when $\mathbf{r}_0 \rightarrow \mathbf{r}_i$. Then, taking the negative of the gradient of $U^{qp} = -\Sigma_i(\mathbf{p}_i\cdot\mathbf{E}_i^q)$ with respect to an ionic position yields

$$\mathbf{F}_i^{qp} = \mathbf{F}_i^{qpI} + \mathbf{F}_i^{qpII} \quad (A.24)$$

$$\mathbf{F}_i^{qpI} = q_i\mathbf{E}_i^{pI} - \sum_{j=1}^{N}\sum_{\mathbf{n}'} q_j[(\mathbf{p}_i\cdot\mathbf{r}_{ij\mathbf{n}})C(\beta,r_{ij\mathbf{n}})\mathbf{r}_{ij\mathbf{n}} - B(\beta,r_{ij\mathbf{n}})\mathbf{p}_i] \quad (A.25)$$

$$\mathbf{F}_i^{qpII} = q_i\mathbf{E}_i^{pII} + \sum_{\mathbf{k}\neq\mathbf{0}} G(\beta,k^2)(\mathbf{p}_i\cdot\mathbf{k})[\cos(\mathbf{k}\cdot\mathbf{r}_i)Q_{\cos}(\mathbf{k}) + \sin(\mathbf{k}\cdot\mathbf{r}_i)Q_{\sin}(\mathbf{k})]\mathbf{k} \quad (A.26)$$

And the negative of the gradient of $U^{pp} = -{}^1/_2\sum_i(\mathbf{p}_i\cdot\mathbf{E}_i^p)$ gives

$$\mathbf{F}_i^{pp} = \mathbf{F}_i^{pp\mathrm{I}} + \mathbf{F}_i^{pp\mathrm{II}} \tag{A.27}$$

$$\mathbf{F}_i^{pp\mathrm{I}} = \sum_{j\neq i}^{N}\sum_{\mathbf{n}}[-(\mathbf{p}_i\cdot\mathbf{r}_{ij\mathbf{n}})(\mathbf{p}_j\cdot\mathbf{r}_{ij\mathbf{n}})D(\beta,r_{ij\mathbf{n}}) + (\mathbf{p}_i\cdot\mathbf{p}_j)C(\beta,r_{ij\mathbf{n}})]\mathbf{r}_{ij\mathbf{n}} + \sum_{j\neq i}^{N}\sum_{\mathbf{n}}[(\mathbf{p}_j\cdot\mathbf{r}_{ij\mathbf{n}})C(\beta,r_{ij\mathbf{n}})\mathbf{p}_i + (\mathbf{p}_i\cdot\mathbf{r}_{ij\mathbf{n}})C(\beta,r_{ij\mathbf{n}})\mathbf{p}_j] \tag{A.28}$$

$$\mathbf{F}_i^{pp\mathrm{II}} = \sum_{\mathbf{k}\neq\mathbf{0}} G(\beta,k^2)[(\mathbf{p}_i\cdot\mathbf{k})\sin(\mathbf{k}\cdot\mathbf{r}_i)P_{\cos}(\mathbf{k}) - (\mathbf{p}_i\cdot\mathbf{k})\cos(\mathbf{k}\cdot\mathbf{r}_i)P_{\sin}(\mathbf{k})]\mathbf{k} \tag{A.29}$$

$$D(\beta,r) = -\frac{1}{r}\frac{\mathrm{d}C(\beta,r)}{\mathrm{d}r} = \left(\frac{8\beta^5}{\sqrt{\pi}}\exp(-\beta^2r^2) + 5C(\beta,r)\right)\frac{1}{r^2} \tag{A.30}$$

Since U^{ind} can be evaluated by eq 2.6, the corresponding Ewald summations are not necessary.

References and Notes

(1) Tasseven, Ç.; Trullàs, J.; Alcaraz, O.; Silbert, M.; Giró, A. *J. Chem. Phys*. **1997**, *106*, 7286.
(2) Vashishta, P.; Rahman, A. *Phys. Rev. Lett.* **1978**, *40*, 1337.
(3) Derrien, J. Y.; Dupuy, J. *Phys. Chem. Liq.* **1976**, *5*, 71.
(4) Inui, M.; Takeda, S.; Shirakawa, Y.; Tamaki, S.; Waseda, Y.; Yamaguchi, Y. *J. Phys. Soc. Jpn.* **1991**, *60*, 3025.
(5) Keen, D. A.; Hayes, W.; McGreevy, R. L. *J. Phys. C: Solid State* **1990**, *2*, 2773.
(6) Andreoni, W.; Tosi, M. P. *Solid State Ionics* **1983**, *11*, 49.
(7) Nield, V. M.; Keen, D. A.; Hayes, W.; McGreevy, R. L. *J. Phys.: Condens. Matter* **1992**, *4*, 6703.
(8) Wilson, M.; Madden, P. A.; Costa-Cabral, B. J. *J. Phys. Chem*. **1996**, *100*, 1227.
(9) Madden, P. A.; Wilson, M. *Chem. Soc. Rev.* **1996**, *25*, 339.
(10) Mayer, J. E. *J. Chem. Phys.* **1933**, *1*, 327.
(11) González, L. E.; González, D. J.; Silbert, M.; Baer, S. *Mol. Phys.* **2001**, *99*, 875.
(12) Hutchinson, F. D. Phil. Thesis, Oxford University, 2000. Hutchinson, F.; Wilson, M.; Madden, P. A. *Mol. Phys.* **2001**, *99*, 811.
(13) Trullàs, J.; Alcaraz, O.; Silbert, M. *J. Non-Cryst. Solids.* To be published.
(14) Waseda, Y. *The Structure of Non-Crystalline Materials*; McGraw-Hill: New York, 1980.
(15) Ahlström, P.; Wallqvist, A.; Engström, S.; Jönsson, B. *Mol. Phys.* **1989**, *68*, 563.
(16) See Hansen, J.-P.; McDonald, I. R. *Theory of Simple Liquids*, 2nd ed.; Academic Press: New York, 1986.
(17) Trullàs, J.; Padró, J. A. *J. Chem. Phys.* **1993**, *99*, 3983.
(18) Vesely, F. J. *J. Comput. Phys.* **1977**, *24*, 361.
(19) Sears, V. F. *Neutron News* **1992**, *3*, 26.
(20) Trullàs, J.; Giró, A.; Silbert, M. *J. Phys.: Condens. Matter* **1990**, *2*, 6643.
(21) Alcaraz, O.; Trullàs, J. *Chem. Phys.* **2000**, *113*, 10635.
(22) Janz, G. J.; Dampier, F. W.; Lakdhminaryanah, G. R.; Lorentz, P. K.; Tomkins, R. P. T. *Molten Salts*; National Bureau of Standards Reference Data Series; Washington, DC, 1968; Vol. 15.
(23) Trullàs, J.; Padró, J. A. *Phys. Rev. B* **1997**, *55*, 12210.
(24) Madden, P. A. *J. Phys.: Condens. Matter* **2000**, *12*, A95.